Evaluating the Contribution of Base Stacking during Translesion DNA Replication†

Edmunds Z. Reineks and Anthony J. Berdis*

Department of Pharmacology and the Comprehensive Cancer Center, School of Medicine, Case Western Reserve University, 10900 Euclid Avenue, Cleveland, Ohio 44106

Received June 3, 2003; Revised Manuscript Received November 12, 2003

ABSTRACT: Despite the nontemplating nature of the abasic site, dAMP is often preferentially inserted opposite the lesion, a phenomenon commonly referred to as the "A-rule". We have evaluated the molecular mechanism accounting for this unique behavior using a thorough kinetic approach to evaluate polymerization efficiency during translesion DNA replication. Using the bacteriophage T4 DNA polymerase, we have measured the insertion of a series of modified nucleotides and have demonstrated that increasing the size of the nucleobase does not correlate with increased insertion efficiency opposite an abasic site. One analogue, 5-nitroindolyl-2′-deoxyriboside triphosphate, was unique as it was inserted opposite the lesion with approximately 1000-fold greater efficiency compared to that for dAMP insertion. Pre-steady-state kinetic measurements yield a k_{pol} value of 126 s^{-1} and a K_d value of 18 μM for the insertion of 5-nitroindolyl-2′-deoxyriboside triphosphate opposite the abasic site. These values rival those associated with the enzymatic formation of a natural Watson−Crick base pair. These results not only reiterate that hydrogen bonding is not necessary for nucleotide insertion but also indicate that the base-stacking and/or desolvation capabilities of the incoming nucleobase may indeed play the predominant role in generating efficient DNA polymerization. A model accounting for the increase in catalytic efficiency of this unique nucleobase is provided and invokes $\pi-\pi$ stacking interactions of the aromatic moiety of the incoming nucleobase with aromatic amino acids present in the polymerase's active site. Finally, differences in the rate of 5-nitroindolyl-2′-deoxyriboside triphosphate insertion opposite an abasic site are measured between the bacteriophage T4 DNA polymerase and the Klenow fragment. These kinetic differences are interpreted with regard to the differences in various structural components between the two enzymes and are consistent with the proposed model for DNA polymerization.

DNA damage can have devastating effects on the integrity and efficiency of diverse biological processes catalyzed inside the cell. In this regard, it is widely recognized that the ability of the DNA polymerase to efficiently replicate damaged DNA can lead to mutagenesis. This ability is commonly referred to as translesion DNA replication (TLR)[1] and is the ultimate cause of various genetic diseases including carcinogenesis (*1*−*3*). Numerous DNA lesions have been identified (reviewed in ref *4*) and demonstrated to be promutagenic (reviewed in refs *5* and *6*). The DNA lesion used in this present study is the abasic site, a commonly formed lesion arising from the hydrolysis of the glycosidic bond between the C1′ of ribose and the N9 of a purine or the N1 of a pyrimidine. Hydrolysis of the glycosidic bond occurs spontaneously (*7*) but can also be enhanced by inappropriate modifications to the various functional groups present on purines (*8*−*10*) and pyrimidines (*11*−*13*). The net effect of this hydrolysis event is that any potential templating information originally present in the DNA is lost. These properties make the abasic site the prototypical nontemplating DNA lesion and an excellent choice to evaluate its effect on the efficiency of DNA polymerization.

Despite the nontemplating nature of the abasic site, most DNA polymerases preferentially insert one of the four natural dNTPs opposite the lesion. For example, the Rev1 polymerase in conjunction with pol ξ has been demonstrated to insert dCMP opposite the abasic site with higher efficiency compared to the other natural nucleotides (*14*). Likewise, the error-prone DNA polymerases, pol η and pol ι, preferentially insert dGMP opposite an abasic site (*15*, *16*). However, these examples do not represent the norm since the vast majority of high-fidelity DNA polymerases preferentially insert dAMP opposite the lesion (*17*−*22*), a phenomenon commonly referred to as the "A-rule".

The mechanistic reason(s) accounting for the A-rule remains (remain) elusive despite numerous kinetic (*17*−*22*), thermodynamic (*23*−*25*), and structural (*26*−*28*) studies performed on abasic-containing DNA. Our efforts have employed steady-state and transient kinetic analyses to determine whether the preferential insertion reflects an enzymatic event associated with enhanced binding affinity

† This research was supported through funding from the Steris Foundation, the American Cancer Society Cuyahoga Unit (021203A), and the American Cancer Society (IRG-91-022-06-IRG) to the Comprehensive Cancer Center at Case Western Reserve University and University Hospitals of Cleveland.

* Corresponding author: telephone, (216) 368-4723; fax, (216) 368-3395; e-mail, ajb15@po.cwru.edu.

[1] Abbreviations: TLR, translesion DNA replication; TBE, Tris-HCl/borate/EDTA; EDTA, ethylenediaminetetraacetic acid sodium salt; dNTP, deoxynucleoside triphosphate; 5-NITP, 5-nitroindolyl-2′-deoxyriboside triphosphate; dDHPTP, dihydropyrimido[4,5-*c*][1,2]oxazin-7-one 2′-deoxyriboside triphosphate; dPTP, pyrene 2′-deoxyriboside triphosphate; N^2-Me-dGTP, N^2-methyl-2′-deoxyriboside triphosphate; gp43 exo$^-$, an exonuclease-deficient mutant of the bacteriophage T4 DNA polymerase.

10.1021/bi034948s CCC: $27.50
Published on Web 12/20/2003

(K_m effect), enhanced catalytic rate (k_{pol} effect), or a combination of both. Using an exonuclease-deficient mutant of the bacteriophage T4 DNA polymerase (gp43 exo$^-$), we demonstrated that the preferential insertion of dAMP is caused by an enhancement in both kinetic parameters (*22*). In this case, gp43 exo$^-$ binds dATP with a 4−34-fold higher affinity than the other dNTPs and also shows a 3−20-fold enhancement in catalytic rate (*22*). Unfortunately, there was not a significant correlation with either enhanced binding affinity or enhanced catalytic rate with the efficiency of insertion of the other three dNTPs. For example, the overall catalytic efficiency for dGMP insertion opposite the abasic site is greater than that for dTMP insertion. However, while the binding affinity for dGTP is 9-fold *higher* than that for dTTP, the rate constant for dGMP insertion is actually 2-fold *slower* than that measured for dTMP insertion. The lack of a direct correlation between the efficiency of insertion and either K_m or k_{cat} values is not unique to the bacteriophage T4 polymerase since similar results have been reported with DNA polymerases isolated from *Escherichia coli* (*17*−*19*) and eukaryotes (*20*, *21*).

One apparent trend, however, is that the larger purines are inserted with a higher overall catalytic efficiency (k_{pol}/K_d) compared to the smaller pyrimidines. In fact, a correlation exists between the measured k_{pol}/K_d values with the relative conformation of the four nucleosides when placed opposite an abasic site (*26*, *27*). Specifically, NMR studies indicate that dAMP exists in a thermodynamically favored intrahelical conformation when placed opposite the lesion (*26*, *27*). This favored conformation correlates well with the relatively high k_{pol}/K_d value for dAMP insertion (*22*). A more convincing argument is that dCMP and dTMP were found to be extrahelical (*26*, *27*), an unfavorable conformation that coincides with their overall poor k_{pol}/K_d values (*22*). These observations led us to propose that the efficiency of nucleotide insertion directly reflects the "stacking" capabilities of the nucleobase (*22*). In this model, we envisioned that once dATP was bound, the polymerase might then overcome the energy barrier associated with insertion easier than the other nucleobases since dAMP appears to be thermodynamically favored inside the helical structure of duplex DNA.

Alternative models have been proposed to account for the efficiency of nucleotide insertion opposite the abasic site lesion (*29*−*31*). A particularly interesting model is that invoking steric constraints and shape complementarity as the predominant forces dictating the efficiency of TLR (*30*, *31*). This model is perhaps best illustrated by the work of Matray and Kool (*31*) demonstrating that pyrene nucleoside triphosphate (dPTP), despite the lack of hydrogen-bonding potential, was inserted opposite the abasic site with a 100-fold higher catalytic efficiency compared to dAMP insertion. Molecular modeling studies indicated that the pyrene·abasic site mispair is roughly the same size and shape of a natural dA·dT base pair (*31*), a result suggesting that the bigger, bulkier pyrene moiety could fill the void present at the abasic site (*31*). The provocative conclusion from this study was that the efficiency of nucleotide insertion (at least opposite an abasic site) is driven by shape complementarity and steric fitting within the defined geometry of duplex DNA (*30*).

We have evaluated these two models by monitoring the enzymatic insertion of a series of modified dNMPs opposite an abasic site using the bacteriophage T4 DNA polymerase. The data from a series of steady-state measurements indicate that simply increasing the size of a nucleobase does not unambiguously increase the rate of DNA polymerization. We have identified one particular nonnatural deoxynucleotide, 5-NITP, that is inserted opposite an abasic site with a 1000-fold higher catalytic efficiency compared to that for the insertion of dAMP. This enhancement occurs despite the similarities in size and shape between 5-NITP and dATP, suggesting that base-stacking and/or desolvation contributions play the predominant role in polymerization efficiency opposite an abasic site. Surprisingly, this enhancement is not observed using the Klenow fragment from *E. coli*. These differences suggest that base stacking and/or desolvation may involve specific and unique interactions within the active site of either DNA polymerase. The kinetic data in conjunction with structural data of various DNA polymerases are interpreted with regard to a model invoking base-stacking contributions from aromatic amino acids lining the active site of the polymerase as well as from intra- and interhelical base-stacking contributions.

MATERIALS AND METHODS

Materials. [γ-^{32}P]ATP and [α-^{32}P]dATP were purchased from New England Nuclear. Unlabeled dNTPs (ultrapure) were obtained from Pharmacia. $MgCl_2$, $Mg(OAc)_2$, and all buffers were from Sigma. Oligonucleotides, including those containing a tetrahydrofuran moiety mimicking an abasic site, were synthesized by Operon Technologies (Alameda, CA). Single-stranded and duplex DNAs were purified and quantified as described (*32*). Nonnatural dNTPs including 5-NITP, dDHPTP, and N^2-Me-dGTP were obtained from TriLink BioTechnologies (San Diego, CA). Each nonnatural dNTP was greater than 99% pure. All other materials were obtained from commercial sources and were of the highest available quality. The exonuclease-deficient mutant of gp43 (gp43 exo$^-$; Asp-219 to Ala mutation) was purified and quantified as previously described (*33*, *34*). The Klenow fragment of *E. coli* DNA polymerase I was purified and quantified as previously described (*35*).

Methods. The assay buffer used in all kinetic studies consisted of 25 mM Tris−OAc (pH 7.5), 150 mM KOAc, and 10 mM 2-mercaptoethanol. All assays, including rapid quench experiments using the instrument described by Johnson (*36*), were performed at 25 °C. Polymerization reactions were monitored by analysis of the products on 20% sequencing gels as described by Mizrahi et al. (*37*). Gel images were obtained with a Molecular Dynamics phosphorimager. Product formation was quantified by measuring the ratio of ^{32}P-labeled extended and nonextended primer. The ratios of product formation are corrected for substrate in the absence of polymerase (zero point). Corrected ratios are then multiplied by the concentration of primer/template used in each assay to yield total product. All concentrations are listed as final solution concentrations.

Comparison of Insertion Efficiency. The efficiency of insertion was evaluated by measuring the extent of elongation of the 13-mer primer to 14-mer. Experiments were performed under single turnover conditions, preincubating 1 μM gp43 exo$^-$ with 250 nM $13/20_{SP}$-mer in the presence of 10 mM Mg^{2+}. The polymerization reaction was then initiated through

the addition of a single, fixed concentration of dNTP. In general, the concentration of dNTP was maintained at K_d levels or 5−10 times the K_d of each dNTP (*22*). Aliquots of the reaction were quenched at various time points through the addition of 200 mM EDTA and processed as described (*22*). Data obtained for single turnover DNA polymerization assays were fit to the equation:

$$y = Ae^{-kt} + C \quad (1)$$

where A is the burst amplitude, k is the first-order rate constant, t is time, and C is a defined constant.

The efficiency of insertion opposite natural template bases was evaluated using pseudo-first-order reaction conditions. In these experiments, 50 nM gp43 exo$^-$ was preincubated with 1000 nM 13/20$_X$-mer in the presence of 10 mM Mg^{2+}. The polymerization reaction was then initiated through the addition of 10 μM dNTP. Aliquots of the reaction were quenched through the addition of 200 mM EDTA at time points ranging from 5 to 600 s and processed as previously described (*22*). To define the steady-state rate of nucleotide insertion, data were fit to the following equation for a straight line:

$$y = mt + b \quad (2)$$

where m is the steady-state rate of dNTP insertion, t is time, and b is the y-intercept at $t = 0$.

Determination of the Kinetic Rate and Dissociation Constants for dNTP Insertion opposite an Abasic Site. gp43 exo$^-$ (1000 nM) was incubated with 250 nM DNA in assay buffer containing EDTA (100 μM) and mixed with variable concentrations of 5-NITP (5−500 μM) and 10 mM $Mg(OAc)_2$. The reactions were quenched with 500 mM EDTA at variable times (0.005−10 s) and analyzed as described above. Data for the dependency of k_{obs} as a function of dNTP concentration were fit to the Michaelis−Menten equation:

$$k_{obs} = k_{pol}[\text{dNTP}]/K_d + [\text{dNTP}] \quad (3)$$

where k_{obs} is the observed first-order rate constant, k_{pol} is the rate of DNA polymerization, K_d is the kinetic equilibrium dissociation constant for dNTP, and dNTP is the concentration of nucleotide substrate.

Pre-Steady-State Nucleotide Incorporation Assays. The time course in 5-NIMP insertion was examined using 13/20$_A$-mer, 13/20$_T$-mer, or 13/20$_{SP}$-mer using a rapid quench instrument employing pseudo-first-order reaction conditions. A preincubated solution of 75 nM gp43 exo$^-$ polymerase and 2000 nM 5′-labeled DNA (final concentrations) was mixed with an equal volume of a solution containing 10 mM $Mg(OAc)_2$ and 25 μM 5-NITP (final concentrations) in the same reaction buffer. The reaction was then terminated at various times by the addition of 500 mM EDTA. Polymerization products were analyzed as described above. Data for each time course were fit to the following equation defining a burst in product formation followed by a steady-state rate:

$$y = Ae^{-kt} + Bt + C \quad (4)$$

where A is the burst amplitude, k is the first-order rate constant, B is the steady-state rate, t is time, and C is a defined constant.

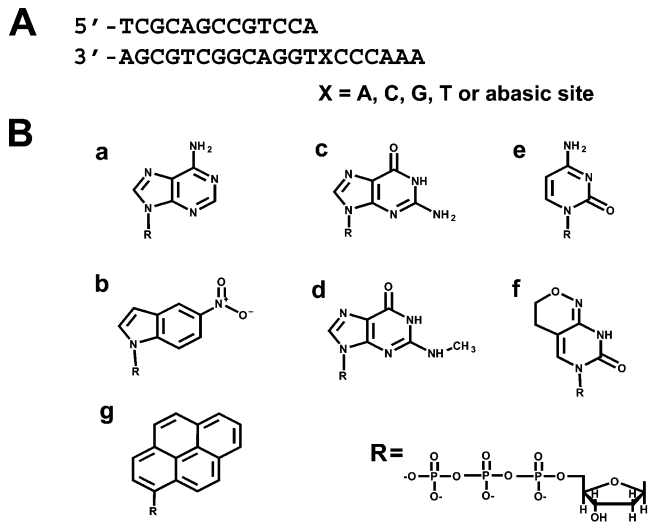

FIGURE 1: (A) DNA substrates used for kinetic analysis. (B) Structures of 2′-deoxynucleoside triphosphates used or referred to in this study are as follows: (a) adenosine, (b) 5-nitroindolyl-2′-deoxyriboside, (c) guanosine, (d) N^2-methylguanosine, (e) cytosine, (f) dihydropyrimido[4,5-*c*][1,2]oxazin-7-one 2′-deoxyriboside (dDHP), and (g) pyrene 2′-deoxyriboside.

RESULTS AND DISCUSSION

Several models have been proposed to account for the preferential insertion of dAMP opposite an abasic site (*17*−*22*, *29*−*31*). In this report, we have quantitatively evaluated the contribution of steric fitting and base stacking to more accurately define the molecular parameters that influence the efficiency of TLR. We attempted to differentiate between these two biophysical parameters by measuring the kinetics of enzymatic insertion of a series of modified dNTPs (Figure 1B) opposite an abasic site, a lesion devoid of hydrogen-bonding potential. A prediction of the steric-fitting model is that the kinetics of dNMP insertion should be influenced by the size of the incoming nucleobase and its ability to fill the "void" left at an abasic site (*31*). Simply put, a larger nucleobase should be inserted opposite the lesion faster than a smaller nucleobase. Alternatively, the efficiency of nucleotide insertion may be relatively independent of nucleobase size and be more dependent upon its base-stacking capabilities.

Nucleotide Survey Analyses. We evaluated the ability of the exonuclease-deficient bacteriophage T4 DNA polymerase, gp43 exo$^-$, to insert unmodified and modified dNTPs opposite an abasic site by measuring the rate of primer elongation, i.e., conversion of 13-mer to 14-mer. To obtain accurate rate constants, experiments were performed under single turnover conditions by preincubating 1 μM gp43 exo$^-$ with 250 nM 13/20$_{SP}$-mer in the presence of 10 mM Mg^{2+} and then initiating the reaction through the addition of a fixed concentration of dNTP.[2] The reactions were quenched through the addition of EDTA at times ranging from 5 to 300 s and then processed as previously described (*22*). Representative data monitoring nucleotide insertion opposite the abasic site is provided in Figure 2. These data demonstrate that both natural and nonnatural nucleotides can be inserted opposite an abasic site. However, qualitative inspec-

Table 1: Summary of Rate Constants for Nucleoside Triphosphate Incorporation opposite an Abasic Site Catalyzed by gp43 Exo$^-$[a]

dNTP	surface area (Å^2)[b]	volume (Å^3)[b]	K_d concn[c] k_{obs} (s^{-1})	$>K_d$ concn k_{obs} (s^{-1})
dATP	255.7	228.7	0.066 ± 0.008 s^{-1}	0.13 ± 0.01 s^{-1}
5-NITP	278.7	260.6	>0.3 s^{-1} [d]	>0.3 s^{-1} [d]
dGTP	264.7	235.5	0.0042 ± 0.0005 s^{-1}	0.011 ± 0.002 s^{-1}
N^2-Me-dGTP	283.2	258.9	0.0099 ± 0.0013 s^{-1}	0.011 ± 0.002 s^{-1}
dCTP	235.8	209.3	0.0032 ± 0.0007 s^{-1}	0.0043 ± 0.0004 s^{-1}
dDHPTP	262.1	245.1	0.0020 ± 0.0004 s^{-1}	0.0025 ± 0.0005 s^{-1}
dPTP	324.9	323.3	ND[e]	ND[e]

[a] Assays were performed using 1000 nM gp43 exo$^-$, 250 nM DNA substrate, 10 mM $Mg(OAc)_2$, and the following concentrations of deoxynucleoside triphosphate: 35 or 350 μM dATP, 35 or 350 μM 5-NITP, 250 or 2500 μM dGTP, 250 or 2500 μM N^2-Me-dGTP, 1000 or 2500 μM dCTP, and 1000 or 2500 μM dDHPTP. [b] The relative surface area and volume for each nucleoside tested in this study were calculated using Spartan '02 software. Although we did not measure the insertion of dPTP opposite an abasic site, the values corresponding to the surface area and volume of pyrene 2′-deoxyriboside are provided for comparison. [c] K_d and $>K_d$ concentration refers to the equilibrium binding constants for the natural dNTPs for insertion opposite an abasic site as previously reported (22). [d] Complete turnover is observed after 5 s. Thus, the value of 0.3 s^{-1} is the maximum value that can be obtained through manual quenching techniques if one assumes a $t_{1/2}$ of 2.5 s. [e] ND = not determined.

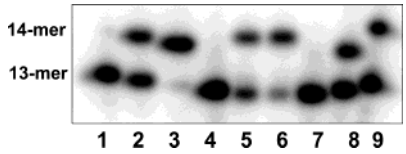

FIGURE 2: Insertion of various nucleoside triphosphates opposite an abasic site. DNA synthesis was monitored using a fixed amount of gp43 exo$^-$ (1000 nM), 13/20SP-mer DNA substrate (250 nM), and variable concentrations of nucleoside triphosphate. The reaction was quenched with 200 mM EDTA, and product formation was analyzed by denaturing gel electrophoresis and quantified by phosphorimaging. Lanes 1, 4, and 7 represent zero time points, i.e., DNA substrate in the absence of added dNTP. Lanes 2 and 3 represent the insertion of 350 μM dATP and 35 μM 5-NITP, respectively, after 120 s. Lanes 5 and 6 represent the insertion of 250 μM dGTP and 250 μM N^2-Me-dGTP, respectively, after 300 s. Lanes 8 and 9 represent the insertion of 1000 μM dCTP and 1000 μM dDHPTP, respectively, after 300 s. Note the difference in mobility of product DNA containing dDHPTP.

tion of the data indicates that the relative size of the nucleotide does not provide a useful predictor for insertion efficiency. Rather, the base-stacking capabilities of the nucleobase appear to play a more predominant role in polymerization efficiency.

This conclusion was quantitatively addressed by comparing the rate constants for insertion. The positive control demonstrates that dAMP is inserted with relatively high efficiency opposite at abasic site (Figure 2, lane 2). At high concentrations of dATP, the observed first-order rate constant (k_{obs}) of 0.13 ± 0.01 s^{-1} reported here (Table 1) is essentially identical to that of 0.15 s^{-1} previously measured under similar reaction conditions (*22*). Although dAMP is preferentially inserted opposite an abasic site, it should be reemphasized that the k_{obs} value for insertion opposite an abasic site is reduced ca. 1000-fold compared to that for insertion opposite T, the normal template base (*22*, *33*, *38*).

A prediction of the steric fit model is that the relatively larger size of N^2-Me-dGTP and dDHPTP (Figure 1 and Table 1) would enhance their rate of insertion opposite the abasic site especially when compared to their unmodified counterparts. In the case of N^2-Me-dGTP, alkylation at the N2 position of guanine increases its size as well as hydrophobicity (*39*). Although N^2-Me-dGMP is inserted opposite an abasic site by gp43 exo$^-$ (Figure 2, lane 6), its efficiency is not enhanced when compared to that for the insertion of dAMP (Figure 2, lane 2). In fact, the k_{obs} of 0.011 s^{-1} measured at high levels of N^2-Me-dGTP is at least 10-fold slower than the rate constant of 0.13 s^{-1} measured using saturating concentrations of dATP (Table 1). Perhaps a more appropriate comparison, however, is made by measuring the insertion of N^2-Me-dGTP with its natural counterpart, dGTP. At lower levels of nucleotide, the rate constant of 0.099 s^{-1} for N^2-Me-dGMP insertion is indeed 2-fold faster than that of 0.045 s^{-1} measured for dGMP insertion (Table 1). This result suggests that steric fitting does indeed influence nucleotide insertion opposite an abasic site. However, identical rate constants are obtained when the concentration of each nucleotide is increased. Although not directly tested, this result suggests that the improved catalytic efficiency for N^2-Me-dGMP insertion is likely caused through an enhancement in binding rather than through a kinetic step associated with phosphoryl transfer.

We next characterized the insertion of dDHPTP opposite the abasic lesion. dDHPTP is a constrained, tautomeric form of cytosine in which addition of an oxime group between the exocyclic amine and C5 of cytosine locks the nucleobase into a keto−imine tautomeric form (*40*) (Figure 1B). We hypothesized that while this modification is distal from the functional groups typically associated with Watson−Crick base pairing, the overall increase in size may enhance the efficiency of insertion. Surprisingly, dDHPMP is poorly inserted opposite the abasic site (Figure 2, lane 9). In fact, at high nucleotide concentrations, the rate for dDHPMP insertion is approximately 2-fold slower than that for dCMP insertion (compare 0.0025 versus 0.0043 s^{-1}). This decrease does not appear to reflect a suboptimal interaction of dDHPTP with gp43 exo$^-$ since the DNA polymerase rapidly inserts dDHPMP opposite a template G or A (A. J. Berdis, unpublished data). Furthermore, gp43 exo$^-$ can easily extend beyond either a dDHPMP·G or dDHPMP·A base pair (A. J. Berdis, unpublished data), indicating that the nonplanar ethoxy portion of the analogue does not adversely affect interactions with either the polymerase or nucleic acid. The data describing the insertion of dDHPMP or N^2-Me-dGMP opposite an abasic site collectively argue that increasing the

[2] To facilitate direct comparison between the insertion kinetics of a modified versus natural dNTP, the concentrations of both were maintained at or above the reported K_d concentration for the natural dNTP (*22*). In this analysis, the K_d for the modified dNTP is assumed to be similar to that of the natural dNTP. Concentrations of dCTP or dDHPTP were maintained at either 1000 ($4 \times K_d$ concentration) or 2500 μM ($10 \times K_d$ concentration) while concentrations of dGTP or N^2-Me-dGTP were maintained at either 250 ($\sim K_d$ concentration) or 2500 μM ($10 \times K_d$ concentration).

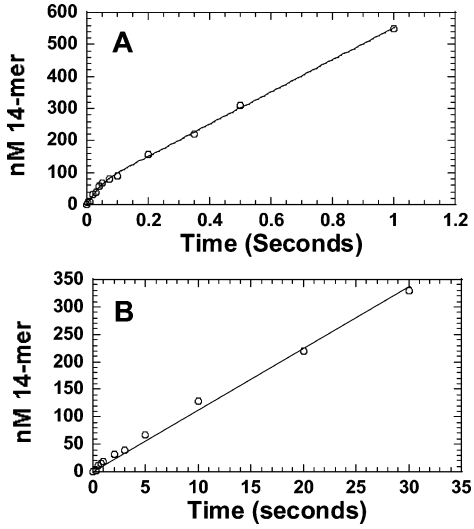

FIGURE 3: Pre-steady state time courses for the insertion of 5-NIMP (A) or dAMP (B) opposite an abasic site. Assays were performed mixing a preincubated solution of 75 nM gp43 exo$^-$ and 2000 nM 5′-labeled DNA with an equal volume of a solution containing 10 mM $Mg(OAc)_2$ and 20 μM 5-NITP or 300 μM dATP in the same reaction buffer (final concentrations). The reaction was then terminated at various times by the addition of 500 mM EDTA at the times demarcated on the graphs. The solid line for 5-NIMP insertion opposite an abasic site was obtained by fitting the data to the kinetic model described in Scheme 1 in which the rate constant for the initial production of DNA_{n+1} (step 3) was maintained at 126 s^{-1} while that for enzyme dissociation (step 7) was maintained at 7 s^{-1}. The solid line for the time course in dAMP insertion opposite an abasic site was obtained using identical analysis except that the rate constant for the initial production of DNA_{n+1} (step 3) was maintained at 0.15 s^{-1}. For insertion of dAMP opposite an abasic site, a value for enzyme dissociation cannot be accurately determined since the time course is linear and limited by the rate constant of 0.15 s^{-1}.

size of the nucleobase does not unambiguously enhance the efficiency of TLR catalyzed by gp43.

We next tested the efficiency of 5-NIMP insertion. Although 5-NITP has a slightly larger surface area and volume compared to dATP (Table 1), the analogue is unique since it is more hydrophobic and is proposed to have stronger "base-stacking" capabilities than natural dNTPs.[3] Indeed, 5-NITP is inserted opposite an abasic site with an extremely high degree of efficiency by gp43 exo$^-$ (Figure 2, lane 3). The apparent rate constant of $\sim$0.3 s^{-1} for 5-NIMP insertion is at least 5-fold faster than that of 0.066 s^{-1} using dATP at an identical concentration (Table 1). The large rate enhancement is not predicted with the steric-fitting model since the size of the 5-NI·abasic site is significantly smaller compared to that of the pyrene·abasic site pair (Figure 1B and Table 1) (*31*). Furthermore, 5-NITP does not simply behave as a dATP anologue since the rate for insertion opposite an abasic site is substantially greater than insertion opposite a natural nucleobase such as T (vide supra).

Transient Kinetic Measurements of 5-NIMP Insertion opposite an Abasic Site. Since the rate of 5-NIMP insertion was relatively fast (k_{obs} greater than 0.3 s^{-1} through manual quenching techniques), experiments were performed using a rapid quench instrument to monitor the kinetics of insertion under pseudo-first-order reaction conditions as previously described (*22*). Under these reaction conditions, the time course in primer extension is biphasic (Figure 3A; see also Scheme 1) and is characterized by a rapid initial burst in elongation followed by a second, slower phase. In contrast, the time course for the insertion of dAMP opposite the abasic lesion is linear and devoid of a burst in product formation (Figure 3B). The biphasic behavior for 5-NIMP insertion is nearly identical to that typically observed during "correct" DNA polymerization such as the insertion of dAMP opposite T (*22*, *33*, *38*). The amplitude of the burst phase represents the first insertion event catalyzed by the DNA polymerase and is likely limited by the conformational change preceding phosphoryl transfer while the second, slower phase is attributed to the release of enzyme from extended DNA.[4] The time course was fit to the equation for a single exponential followed by a steady-state phase (eq 4). This analysis provides a burst amplitude of 70 $\pm$ 6 nM, a value equivalent to the concentration of enzyme used in the experiment (75 nM). In addition, the rate constant for the burst phase (k_{obs}) is 27.7 $\pm$ 7.3 s^{-1} while a k_{cat} value of 7.1 $\pm$ 0.1 s^{-1} (obtained by dividing the steady-state rate by the burst amplitude) is measured. It is interesting to note that the k_{cat} value of 7.1 s^{-1} is nearly 3.5-fold faster than the value of $\sim$2 s^{-1} measured for precise DNA synthesis (*33*, *38*). Values for the burst amplitude, k_{obs}, and k_{cat} are provided in Table 2.

Single turnover conditions were then employed to accurately measure the kinetic dissociation constant, K_d, as well the maximal polymerization rate, k_{pol}, for 5-NIMP insertion

Scheme 1: Minimal Kinetic Mechanism for the Bacteriophage T4 DNA Polymerase[a]

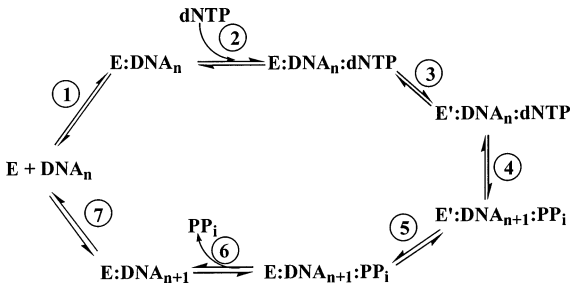

[a] Individual steps along the pathway for DNA polymerization are numbered and identified as follows: step 1 represents E binding to DNA, step 2 represents binding of dNTP to the E·DNA complex, step 3 represents the conformational change preceding phosphoryl transfer, step 4 represents the phosphoryl-transfer step, step 5 represents the conformational change following phosphoryl transfer, step 6 represents the release of PP_i, and step 7 represents E dissociation from product DNA. Abbreviations: E = gp43 exo$^-$, DNA_n = DNA substrate, E′ = conformational change in gp43 exo$^-$, PP_i = inorganic phosphate, and DNA_{n+1} = DNA product (DNA extended by one nucleobase).

[3] The base-stacking properties of 5-nitroindole are based primarily upon the demonstration that the introduction of 5-nitroindole into duplex DNA increases the thermostability of the DNA despite the lack of hydrogen-bonding capabilities of the nonnatural nucleoside (*41*). Likewise, 5-nitroindole is substantially more hydrophobic than natural nucleobases such as adenine and guanine (*42*).

[4] The biphasic time course is consistent with data obtained measuring correct insertion of a natural dNMP opposite its complementary partner (*33*, *38*). Under normal replication conditions, it has been established that the burst phase is limited by the conformational change while the steady-state phase is limited by release of polymerase from extended DNA. We note that the biphasic time course measured using 5-NIMP insertion is consistent with this interpretation but is not proof. Other approaches such as isotope trapping and/or spectroscopic measurement of the conformational change and product release steps are needed to truly validate this conclusion.

Table 2: Summary of Pre-Steady-State Kinetic Rate Constants Measured for 5-NIMP Insertion opposite an Abasic Site or Natural Nucleobase[a]

DNA substrate	amplitude (nM)	k_{obs} (s^{-1})	steady-state rate (nM/s)	k_{cat} (s^{-1})
$13/20_{SP}$-mer	70 ± 6	27.7 ± 7.2	502 ± 10	7.1 ± 0.1
$13/20_{A}$-mer	69 ± 14	0.57 ± 0.15	13.5 ± 1.6	0.20 ± 0.01
$13/20_{C}$-mer	ND[b]	NA[c]	9.3 ± 0.5	0.12 ± 0.01
$13/20_{G}$-mer	ND	NA	3.5 ± 0.03	0.047 ± 0.008
$13/20_{T}$-mer	67 ± 6	0.48 ± 0.11	2.3 ± 0.3	0.034 ± 0.004

[a] Assays were performed using 75 nM gp43 exo$^-$, 2000 nM DNA substrate, and 25 μM 5-NITP in the presence of 10 mM $Mg(OAc)_2$. [b] ND = not detected. [c] NA = not applicable.

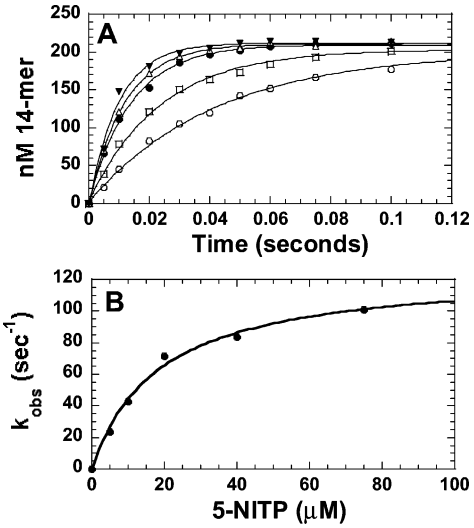

FIGURE 4: Dependency of 5-NITP concentration on the apparent burst rate constant as measured under single turnover conditions. (A) gp43 exo$^-$ (1000 nM) and 5′-labeled 13/20SP-mer (250 nM) were preincubated, mixed with increasing concentrations of Mg^{2+}• 5-NITP to initiate the reaction, and quenched with 500 mM EDTA at variable times (0.005−0.25 s). The incorporation of 5-NITP was analyzed by denaturing gel electrophoresis. 5-NITP concentrations were 5 μM (○), 10 μM (□), 20 μM (●), 40 μM (△), and 75 μM (▼). The solid lines represent the fit of the data to a single exponential. (B) The observed rate constants for 5-NIMP insertion (●) were plotted against 5-NITP concentration and fit to the Michaelis−Menten equation to determine values corresponding to K_d and k_{pol}.

opposite the abasic site. Maintaining enzyme in molar excess versus DNA substrate alleviates complications arising from any kinetic step after phosphoryl transfer and allows for the measurement of the kinetic steps reflecting initial ground-state binding of dNTP, the conformational change prior to chemistry, and/or the chemistry step itself.

Figure 4A displays the dependence on the rate of enzymatic incorporation on the concentration of 5-NITP. All time courses are best defined as a single exponential process and were fit to eq 1 to define k_{obs}, the rate constant of product formation. The plot of k_{obs} versus 5-NITP concentration is hyperbolic (Figure 4B). A fit of the data to the Michaelis−Menten equation yields a k_{pol} value of 126 ± 6 s^{-1}, a K_d value of 18 ± 3 μM, and a k_{pol}/K_d value of 7×10^6 M^{-1} s^{-1} (Table 3). The overall catalytic efficiency for inserting 5-NIMP opposite an abasic site is 1600-fold higher than that for dAMP insertion opposite the same lesion (compare 4.3×10^3 with 7×10^6 M^{-1} s^{-1}) (*22*). The increase in catalytic efficiency is not caused by an enhancement in binding affinity for 5-NITP since the K_d for 5-NITP is only 2-fold

Table 3: Summary of Kinetic Rate and Equilibrium Constants for the Incorporation of 5-NITP Catalyzed by gp43 Exo$^-$ [a]

DNA substrate	k_{pol} (s^{-1})	K_d (μM)	k_{pol}/K_d (M^{-1}/s^{-1})
$13/20_{SP}$-mer	126 ± 6	18 ± 3	7.00×10^6
	(−4.0 kcal/mol)[b]	(−0.4 kcal/mol)	(−4.4 kcal/mol)
	(−0.14 kcal/mol)[c]	(+0.35 kcal/mol)	(+0.21 kcal/mol)
$13/20_{A}$-mer	4.4 ± 0.1	23 ± 2	1.91×10^5
	(+1.85 kcal/mol)[c]	(+0.47 kcal/mol)	(+2.32 kcal/mol)
$13/20_{C}$-mer	0.13 ± 0.02	36 ± 19	3.61×10^3
	(+3.94 kcal/mol)	(+0.76 kcal/mol)	(+4.7 kcal/mol)
$13/20_{G}$-mer	0.12 ± 0.01	10 ± 5	1.20×10^4
	(+3.98 kcal/mol)	(0 kcal/mol)	(+3.98 kcal/mol)
$13/20_{T}$-mer	0.9 ± 0.1	9.0 ± 0.8	1.91×10^5
	(+2.80 kcal/mol)	(+0.07 kcal/mol)	(+2.73 kcal/mol)

[a] Assays were performed using 1000 nM gp43 exo$^-$, 250 nM DNA substrate, and variable concentrations of 5-NITP in the presence of 10 mM $Mg(OAc)_2$. [b] $\Delta\Delta G^‡$ values were calculated using the equation $\Delta\Delta G^‡ = RT \ln K$, where $R = 1.9872$ cal/mol^{-1} K^{-1}, $T = 298$ K, and K is the ratio of respective kinetic equilibrium or rate constants, i.e., k_{5-NITP}/k_{dATP}. In this instance, the values of K were determined comparing the rate and kinetic equilibrium constants for the enzyme-catalyzed insertion of 5-NIMP versus dAMP opposite an abasic site. [c] $\Delta\Delta G^‡$ values represent the comparison for insertion of 5-NIMP opposite the natural nucleobase versus insertion of the correct dNMP opposite its corresponding Watson−Crick base pair partner. A k_{pol} of 100 s^{-1} and a K_d of 10 μM as measured for the insertion of dATP opposite T (*33*, *38*) were used for all other natural Watson−Crick base pairs.

lower than that measured for dATP (compare 18 versus 35 μM, respectively). Instead, there is nearly a 1000-fold enhancement in the polymerization rate constant for 5-NIMP insertion compared to that for dAMP (126 versus 0.15 s^{-1}, respectively). Surprisingly, the k_{pol}/K_d value of 7×10^6 M^{-1} s^{-1} for the enzymatic formation of a 5-NI•abasic site pair is nearly identical for an A•T base pair [10^7 M^{-1} s^{-1} (*33*, *38*)]. The incredible efficiency of 5-NIMP insertion opposite the abasic site again reemphasizes that hydrogen bonds need not entirely account for efficient DNA polymerization (*43*, *44*).

Direct comparison of the k_{pol}/K_d values measured for 5-NITP and dATP provided in Table 3 allows us to quantitatively evaluate the change in relative free energy ($\Delta\Delta G^‡$) associated with the overall enhancement in nucleotide insertion. $\Delta\Delta G^‡$ values were calculated using the equation: $\Delta\Delta G^‡ = RT \ln K$, where $R = 1.9872$ cal mol^{-1} K^{-1}, $T = 298$ K, and K is the ratio of respective kinetic equilibrium or rate constants, i.e., k_{5-NITP}/k_{dATP}. This analysis reveals that most of the favorable change in free energy is achieved presumably during the conformational change step (−4.0 kcal/mol) rather than in ground-state binding of the nucleotide (−0.4 kcal/mol).

Kinetics of 5-NIMP Insertion opposite Natural Nucleobases. The efficiency of 5-NIMP insertion opposite the four natural bases was next measured to evaluate the contribution of hydrogen-bonding potential as well as steric fitting toward catalysis. It was predicted that 5-NIMP should be preferentially inserted opposite T and C since it mimics the relative size and shape of a purine. The kinetic parameters obtained using single turnover reaction conditions (Table 3) provide evidence that this prediction is not entirely accurate. While the high catalytic efficiency for 5-NIMP insertion opposite T is expected, the high efficiency for insertion opposite A is counterintuitive since this forms a purine•purine-like base pair that should be unfavorable. In contrast, the overall

catalytic efficiency for insertion opposite C is surprisingly low and is not predicted by the steric fit model. In fact, the low efficiency for insertion opposite C is nearly identical to that for the insertion of 5-NIMP opposite G, a base pair that is predicted to be unfavorable. The inability to directly correlate the kinetic efficiency of insertion with the shape and/or geometry of the base pair detracts from the importance of steric fitting during nucleotide insertion catalyzed by gp43 exo$^-$. Surprisingly, the differences in catalytic efficiency are not caused by dramatic alterations in ground-state binding since the K_d for 5-NITP remains relatively independent of nucleobase composition. Instead, the kinetic parameter that varies more significantly is the k_{pol} value. These data collectively indicate that 5-NITP is "universal" with regard to ground-state binding but not universal with respect to mediating the potential conformational change in the enzyme−nucleic acid complex necessary for catalysis.

The $\Delta\Delta G^{\ddagger}$ values associated with insertion of 5-NIMP opposite any of the four natural bases provide unique insight into the dynamics of base pair formation (Table 3). The $\Delta\Delta G^{\ddagger}$ values are increased by +2.3 to +4.7 kcal/mol relative to the enzymatic formation of an A·T base pair. In all cases, the change in free energy is dominated by the conformational change or phosphoryl-transfer step rather than simple perturbations in ground-state binding. The differences in free energy could actually reflect steric hindrance by the bulkier nitro moiety during insertion opposite natural bases. While this mechanism undoubtedly accounts for some of the decrease in efficiency, it cannot account for its entirety for two reasons. First, 5-NITP is a purine analogue that is not preferentially inserted opposite the pyrimidines, T and C, as predicted by steric fit. Second, removal of the nitro moiety actually reduces the rate of insertion opposite any of the four natural nucleobases (Xuemei Zhang, Irene Lee, and A. J. Berdis, unpublished data), a result inconsistent with simple steric hindrance induced by the nitro moiety.

What Is the Rate-Limiting Step for Enzymatic Insertion of 5-NIMP opposite Natural Nucleobases? Time courses in 5-NIMP insertion opposite any of the four natural bases were generated under pseudo-first-order conditions to further evaluate the dynamics of insertion. This analysis was essential since the k_{pol} values of 1 and 4 s^{-1} measured under single turnover conditions for insertion opposite T and A, respectively, are similar in magnitude to the rate constant typically measured for polymerase dissociation from product DNA (*33*, *38*). The similarities in rate constants made it impossible to identify if product release or a kinetic step preceding product release is rate-limiting for enzyme turnover. Biphasic time courses are observed for 5-NIMP insertion opposite T or A (Supporting Information, Figure 1) and clearly indicate that a step after phosphoryl transfer is rate-limiting for enzyme turnover. On the basis of the similarities in the time courses obtained during correct dNMP insertion (*22*, *33*, *38*), we presume the fast phase of initial product formation most likely represents the conformational change preceding phosphoryl transfer. However, we note that this step may indeed be phosphoryl transfer. Regardless, each time course was fit to eq 4 to provide values corresponding to the burst amplitude, k_{obs}, and k_{cat} (Table 2). Nearly identical burst amplitudes of 69 and 67 nM were obtained for 5-NIMP insertion opposite A and T, respectively. These values are consistent with the burst amplitude measured for insertion of the analogue opposite the abasic site. A k_{obs} of 0.57 ± 0.15 s^{-1} and a k_{cat} of 0.20 ± 0.01 s^{-1} were measured for insertion opposite A while a k_{obs} of 0.48 ± 0.15 s^{-1} and a k_{cat} of 0.034 ± 0.005 s^{-1} were measured for insertion opposite T. The low k_{obs} values reflect the utilization of subsaturating concentrations of 5-NITP in each experiment. It is interesting to note that, in both cases, the k_{cat} values of 0.20 s^{-1} and 0.034 s^{-1} are much slower than the k_{cat} of ∼2 s^{-1} measured during proper DNA replication, i.e., formation of a natural Watson−Crick base pair (*33*, *38*). A possible explanation for these slower k_{cat} values is that the release of enzyme from product DNA (DNA_{n+1}) is influenced by the nature of the formed nonnatural base pair. Alternatively, these decreases may reflect the accumulation of a nonproductive ternary complex composed of gp43·DNA_{n+1}·5-NITP. These nonproductive complexes may indeed exist since 5-NITP appears to bind indiscriminately opposite natural template bases (Table 3) and is an effective chain terminator of DNA synthesis catalyzed by gp43 exo$^-$ (A. J. Berdis, unpublished data).

The linear time courses observed for 5-NIMP insertion opposite C or G (Supporting Information, Figure 2) directly contrast the biphasic time courses observed for the insertion opposite A and T. The lack of a defined burst suggests that phosphoryl transfer or the conformational change preceding phosphoryl transfer is completely rate-limiting for enzyme turnover. Fits of the data to eq 2 provided k_{cat} values of 0.047 ± 0.008 s^{-1} and 0.12 ± 0.01 s^{-1}, respectively. Collectively, these data indicate that the rate-limiting step for polymerase turnover using 5-NITP is dependent upon the "pairing" partner for 5-nitroindole.

Comparison between DNA Polymerases. The steric fit model postulates that constraints in the size and geometry of the formed base pair play the predominant role in dictating the efficiency of nucleotide insertion. Accordingly, this model predicts that the formation of a base pair is guided by its potential thermodynamic stability rather than through kinetic control imposed by the enzyme. This infers that the kinetics of nucleotide insertion should be directly linked to the sequence/structure of the nucleic acid and be relatively insensitive to the DNA polymerase used to catalyze its insertion. Comparing the efficiency of 5-NIMP insertion opposite an abasic site using the same DNA substrate but employing different DNA polymerases tested this model. In these experiments, steady-state rates of nucleotide incorporation were measured using either 100 nM gp43 exo$^-$ or 100 nM Klenow fragment, 1000 nM $13/20_{SP}$-mer, 10 mM Mg^{2+}, and a fixed concentration of deoxynucleoside triphosphate (100 μM). As summarized in Table 4, it is apparent that both gp43 exo$^-$ and the Klenow fragment display similar trends in catalytic efficiency for natural dNMP insertion opposite the abasic site, i.e., dA > dG > dC, dT. While these data are consistent with previously published results (*17*, *18*, *30*), closer inspection of the data provides two striking observations. First, the Klenow fragment inserts dAMP opposite an abasic site with an approximately 10-fold faster rate than does gp43 exo$^-$. Perhaps more surprising, however, is the relatively slow rate by which the Klenow fragment inserts 5-NIMP opposite an abasic lesion. In fact, the insertion of 5-NIMP is at least 4-fold slower as compared to the insertion of dAMP. These data directly contrast that obtained with gp43 exo$^-$ in which 5-NIMP is inserted 20-fold faster under

Table 4: Comparison of Rates for Nucleoside Triphosphate Incorporation opposite an Abasic Site Catalyzed by Bacteriophage T4 gp43 Exo$^-$ or the Klenow Fragment of *E. coli* DNA Polymerase I[a]

dNTP	gp43 exo$^-$ rate (nM/s)	Klenow fragment rate (nM/s)
dATP	9.4	>100
dCTP	0.12	0.19
dGTP	0.49	1.4
dTTP	0.38	0.09
5-NITP	>200	24

[a] Assays were performed using 100 nM gp43 exo$^-$ or 100 nM Klenow fragment, 1000 nM $13/20_{SP}$-mer, 10 mM $Mg(OAc)_2$, and 100 μM dNTP or 100 μM 5-NITP.

identical reaction conditions. The slower rate of 5-NIMP insertion by the Klenow fragment may be caused by potential perturbations in ground-state binding, phosphoryl transfer, or any conformational changes flanking phosphoryl transfer. We are currently performing rigorous, quantitative analyses to more accurately evaluate these issues. Regardless, the large differences in rates indicate that the efficiency of insertion is not mediated solely by thermodynamic stability of the formed nucleobase pairs or nucleic acid composition. Although these DNA polymerases share similarities in the overall kinetic mechanism, there probably exist subtle differences in the dynamics of the various kinetic steps associated with efficient DNA polymerization. An intriguing possibility is that steric fit plays a large role in polymerization efficiency catalyzed by the Klenow fragment but plays a minor role during catalysis by gp43. Indeed, a recent report by Chiaramonte et al. (*45*) demonstrates that the Klenow fragment inserts dAMP opposite an abasic site with a higher efficiency than 5-NIMP. These authors conclude from these and other results that the efficiency of DNA polymerization may be mediated by virtue of a negative selection mechanism rather than by steric fit (*45*). There is accumulating evidence that different DNA polymerases appear to invoke different catalytic strategies such as steric fit, base stacking, and negative selection to facilitate efficient dNMP insertion (*45*−*48*).

A New Model for Polymerization Efficiency during Nucleotide Insertion? It is well established that the double-helical nature of duplex DNA is stabilized by both enthalpic and entropic contributions (*49*−*51*). The negatively charged phosphate backbone of DNA provides an enthalpic stabilizing force while the hydrophobic interior of the helix provides entropic stabilization through nucleobase stacking as well as through desolvation. While the nucleobases on opposite strands are paired with their corresponding partner through hydrogen-bonding interactions, most of the stability of the helix is proposed to result from the slightly out of plane stacking of the nucleobases on "top" of each other. Indeed, several DNA structures provide evidence that the helical twist of the DNA requires that the stacked nucleobases be offset (*51*), a conformation that allows a nucleobase to be in direct $\pi-\pi$ contact with its 3′ and 5′ neighbors. In fact, the distance separating the planes of the nucleobase is ~3.4 Å, a distance corresponding to the thickness of the π-electrons in an aromatic ring. In this regard, it is easy to envision that the aromatic nature and conjugated π-electron system of 5-nitroindole would substantially add to its thermodynamic stabilization inside the helical confines of duplex DNA. In this case, the enhanced rate of 5-NIMP insertion would be facilitated by these entropic factors.

However, questions remain as to how 5-NITP is transferred from the hydrophilic environment of bulk solvent into the hydrophobic environment of the DNA. Specifically, what role does the DNA polymerase play in mediating this transfer? Several enzymatic steps including nucleotide binding, conformational changes, and phosphoryl transfer could potentially affect nucleobase transfer. To gain more insight into this process, we have attempted to correlate the kinetic behavior of 5-NIMP insertion with the known structures of various DNA polymerases. While no structures have been solved for full-length gp43 from bacteriophage T4, there exist several structures of the homologue from the related organism, bacteriophage RB69 (*52*−*54*). The DNA polymerases from T4 and RB69 possess ~60% sequence identity (*52*), and both enzymes are similar in function and presumably tertiary structure since either enzyme can substitute for the other to perform in vivo replication (*56*).

The overall structure of gp43 is similar to that of other DNA polymerases as it contains the hallmark "fingers", "thumb", and "palm" subdomains (reviewed in ref *57*). The most conserved structural region in all DNA polymerases characterized to date is the palm subdomain which contains the three conserved carboxylic acids involved in the chemistry of phosphoryl transfer (*58*). The thumb domain predominantly interacts with the duplex DNA while the fingers domain contains most of the amino acids that interact with the incoming dNTP (*54*). A point that will be discussed later is the fact that the fingers and thumb domains of gp43 differ from those of other well-characterized DNA polymerases including the Klenow fragment from *E. coli* (*58*, *59*) and the bacteriophage T7 DNA polymerase (*60*, *61*). Close inspection of the active site of gp43 reveals two other regions containing conserved residues of distinct chemical function. These include a cluster of positively charged amino acids (K560, R482, and K486) and a cluster of aromatic residues (Y416, Y567, and Y391)[5,6] (*52*−*54*). The role of these clusters in DNA polymerization is implicated through postulated movements in the domains of gp43. These movements were generated through comparison of the structures of gp43 in the apoenzyme form (*52*), in complex with DNA (the "editing" complex) (*53*), and in complex with a dideoxy-terminated DNA and complementary dNTP (the "polymerization" complex) (*54*). We argue that the cluster of aromatic amino acids plays an important role in providing entropic stabilization during dNTP binding as well as in dNMP insertion into DNA. Existing structural data suggest that the incoming dNTP binds to the open conformation of the polymerase at the fingers subdomain (*51*). The binding of the correct dNTP to the polymerase−DNA complex then induces a rotation of the fingers subdomain that possibly reflects the conformational change step that is observed kinetically (*38*, *52*, *54*). The dynamics of this rotation appear critical for catalysis since this motion also moves the cluster of positively charged amino acids, K560, R482, and K486,

[5] Molecular modeling studies indicate that the 5-nitro group of 5-nitroindole is not zwitterioinic as commonly denoted but instead adds to the conjugated π-electron system of the indole ring.

[6] Y391, Y416, and Y567 in gp43 from bacteriophage RB69 are equivalent to F388, Y413, and Y564 in gp43 from bacteriophage T4 (*58*).

closer to the active site where they interact predominantly with the triphosphate groups of the incoming dNTP as opposed to the functional groups on the nucleobases. This rotation creates the "closed" conformation that presumably aids to orient the 3′-hydroxyl of the primer for an in-line attack on the α-phosphorus atom of the bound dNTP (*54*).

In the structure of gp43, there is a lack of any observable electrostatic or hydrogen-bonding interactions with the formation of the nascent base pair (*54*). This observation was originally proposed to reflect the size constraints of a correct versus incorrect base pair (*54*). Although some of the kinetic data presented here are consistent with this steric fit mechanism, we propose an alternative model in which the binding of the incoming dNTP is mediated by the favorable $\pi-\pi$ interactions of the aromatic nucleoside with the cluster of aromatic residues including Y416, Y567, and Y391 lining the active site. Y567 is one of the most highly conserved residues in the fingers subdomain of all DNA polymerases (*62*). This tyrosine is positioned near the catalytic site of the polymerase at the end of helix P of the fingers domain and is proposed to "sense" the geometry of the newly formed base pair (*62*). This amino acid plays an important role in dNTP discrimination since substitution with smaller amino acids reduces the overall fidelity of gp43 (*60*, *61*). Y416 is another highly conserved amino acid (*65*) that appears to be primarily involved in dNTP/rNTP discrimination (*65*). While the hydroxyl group is proposed to provide a "steric gate" preventing the insertion of rNTPs, closer inspection reveals that portions of the incoming dNTP also stack on top of the phenyl ring of Y416 (*54*). This stacking feature may contribute to entropic stabilization of binding the correct base pair.

Three other tyrosine residues, Y619, Y626, and Y708, are within 14 Å of the primer/template junction and could also participate in $\pi-\pi$ stacking interactions with DNA and/or the incoming dNTP. In fact, it is quite intriguing that Y619 and Y626 in gp43 can be accurately aligned with Y181 and Y188 in HIV-RT (*66*) since these residues in HIV-RT form part of the binding site for hydrophobic and aromatic nonnucleoside inhibitors such as nevirapine (*67*). It is unknown if nonnucleoside inhibitors such as nevirapine also inhibit gp43.

We have demonstrated that, despite the use of identical reaction conditions, the Klenow fragment inserts 5-NIMP opposite an abasic site at a 4-fold slower rate compared to gp43 exo$^-$. We propose that the kinetic differences reflect subtle structural differences between the two enzymes. Indeed, a recent report highlights the differences in kinetic behavior between gp43 from RB69 and the Klenow fragment with the observed differences in the structures of dNTP binding sites (*68*). Specifically, Li et al. (*66*) proposed that binding of the incoming dNTP is mediated first by the fingers domain interacting with the triphosphate groups of the incoming dNTP. Following this initial binding, there is a conformational change in which the fingers rotate toward the palm subdomain to place the incoming dNTP in the active site of the polymerase. It should be noted that the Klenow fragment has several aromatic amino acids including Y766 and F762 that are equivalent to those present in gp43 from phage T4 and RB69 (*62*). However, these aromatic amino acids move significantly during the transition from the open to the closed conformation in the Klenow fragment (*68*). This observation directly contrasts that of the movements detected in gp43 and implies that the Klenow fragment does not have a preorganized dNTP binding site as does gp43 (*68*). It is tempting to speculate that the measurable differences in the rate of 5-NIMP insertion between the two enzymes reflect alterations associated with the conformational change step. Further experimentation is clearly required to evaluate this hypothesis.

The data from our kinetic studies in conjunction with the structural information allows us to propose the model summarized in Figure 5. In this model, the DNA polymerase is bound to the DNA containing an abasic site and is poised for polymerization. In this binary complex, there exists a "nonspecific" dNTP binding pocket lined with aromatic amino acids such as Y416 and Y567 (*54*). We propose that these aromatic moieties provide a hydrophobic environment for initial $\pi-\pi$ stacking interactions with the aromatic moiety of an incoming nucleotide (step A). The significance of this interaction is to provide an entropic trap which stabilizes the binding of the incoming dNTP with the polymerase−DNA complex. The importance of the proposed entropic trap becomes obvious when one considers the necessity for desolvation of the incoming nucleobase as well as the requirement for transfer of the nucleobase into the helix. Binding of dNTP is then followed by the movement of the fingers subdomain, i.e., the conformational change preceding phosphoryl transfer, which places the triphosphate moiety in close proximity with the positively charged amino acids such as K560 and R482 (step B). Concomitant with the movement of the triphosphate moiety is the "flipping" or base-stacking step in which the nucleobase portion of the incoming dNTP is transferred from the hydrophobic environment of the tyrosine-lined binding site into the hydrophobic environment of the interior of the duplex DNA (step B). The placement of the nucleobase from one hydrophobic environment into another is likely to be energetically favorable and could provide the driving force for polymerization as well as be involved in the maintenance of fidelity. The movements associated with this conformational change also act to polarize the α-phosphate group for nucleophilic attack by the 3′-hydroxyl of the primer, a step required for phosphoryl transfer and elongation of the primer strand (step C).

An alternative mechanism initially suggested by an anonymous reviewer of this paper is that the high catalytic efficiency for 5-NIMP insertion opposite an abasic site reflects an enhanced effect on desolvation rather than base stacking. The role of desolvation is perhaps best exemplified by first examining correct nucleotide insertion prior to discussing translesion DNA synthesis. During correct DNA replication, proper base pairs are formed within the helix of the DNA. Prior to their formation, however, there is a significant entropic penalty since the functional groups of the incoming dNTP must be desolvated. After desolvation, the incoming dNMP is stabilized within the helix of the duplex by enthalpic contributions, i.e., the formation of hydrogen-bonding interactions with the template base, as well as by other entropic factors including base stacking. The abasic site, however, provides a unique situation as the inability to form hydrogen bonds places additional energetic demands on catalysis since the contribution from enthalpic stabilization is greatly diminished. Therefore, the ability of a natural nucleobase such as dAMP to exist opposite the

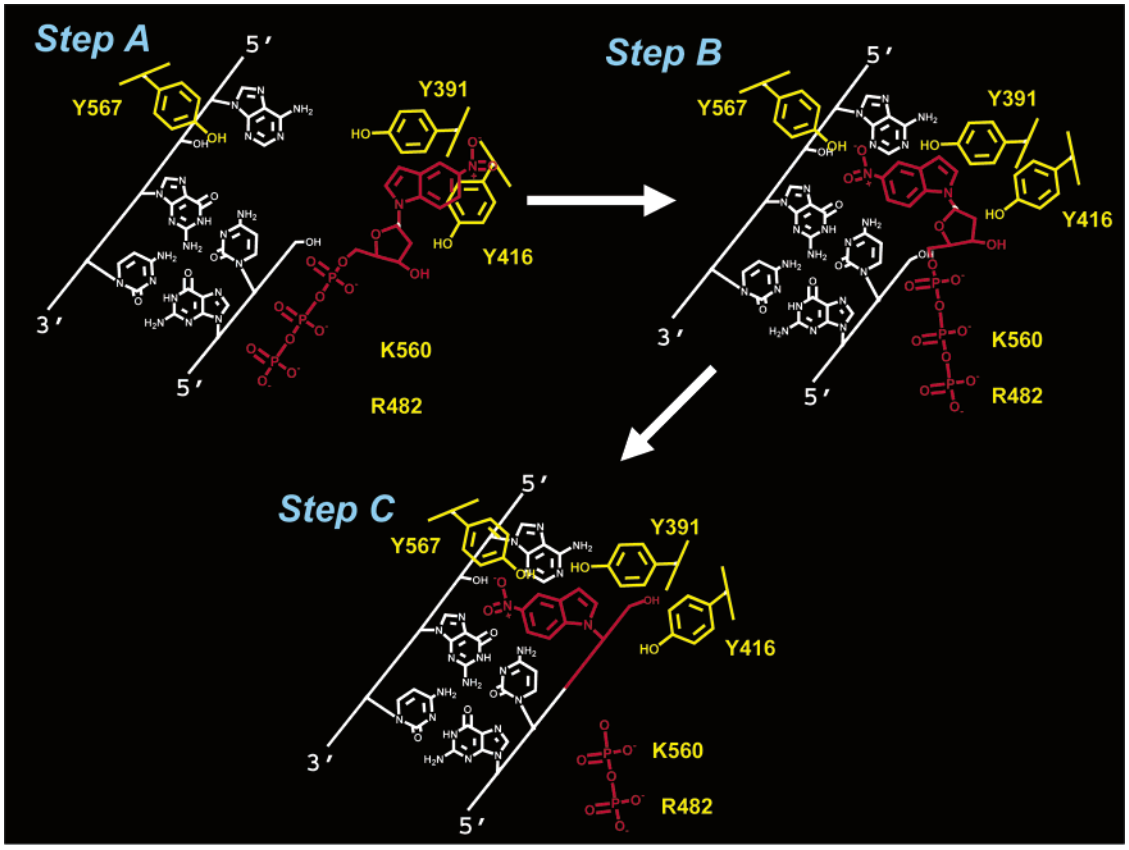

FIGURE 5: Proposed model for the enzymatic insertion of 5-NIMP insertion opposite an abasic site. Step A represents the binding of dNTP into the putative nonspecific binding pocket lined with aromatic amino acids. Step B represents the conformational change preceding phosphoryl transfer required to place the triphosphate moiety in close proximity with the positively charged amino acids as well as to stack the nucleobase portion of the incoming dNTP into the hydrophobic environment of the interior of the duplex DNA. Step C represents the phosphoryl-transfer step required for elongation of the primer strand. For convenience, nucleic acid is colored white, amino acids in the DNA polymerase's active site are colored yellow and labeled according to the numbering system of gp43 from bacteriophage RB69, and 5-NITP is colored red.

abasic site becomes much more dependent on the change in free energy associated with desolvation. Indeed, the slow kinetics of dNMP insertion could reflect this unfavorable condition. In contrast, 5-NIMP is inserted more effectively because the analogue is already highly desolvated. In fact, the calculated oil-to-water partition coefficient for 5-nitroindole is +2.46 while that for adenine and guanine are −1.07 and −1.36, respectively (*42*). As such, the nucleobase may be stabilized within the interior of DNA because the energetic penalty from desolvation is considerably less. We are currently evaluating the proposed role of desolvation during DNA polymerization by performing a structure−activity relationship analysis on various 5-substituted indole deoxyriboside triphosphates.

Conclusions. We have quantitatively evaluated the contribution of base stacking and steric fit as two interrelated biophysical parameters that can account for nucleotide insertion opposite an abasic site. Data obtained with gp43 exo$^-$ indicate that the relative size of the incoming nucleobase plays a minor role in mediating efficient insertion. Instead, we demonstrate that 5-NITP, a novel nucleobase with enhanced base-stacking and hydrophobic characteristics compared to natural dNTPs, is inserted opposite an abasic site with a 1000-fold greater overall catalytic efficiency compared to dATP. During translesion DNA synthesis, 5-NIMP is inserted with a fast k_{pol} value of 126 s^{-1} and binds to the polymerase−DNA complex with relatively high affinity (K_d = 18 μM). Collectively, these values indicate that the catalytic efficiency for the formation of a 5-NI·abasic site is nearly identical to that for a correct A·T base pair (compare 0.7×10^7 with 10^7 M^{-1} s^{-1}) (*33*, *38*). In fact, 5-NIMP is inserted opposite an abasic site with at least 10-fold greater efficiency compared to dPTP, the molecule reported to be the "specific partner" for an abasic site (*31*). Again, this enhancement during translesion DNA replication occurs despite the smaller size of 5-NI compared to that of pyrene, suggesting that base stacking and/or desolvation may play the predominant role in polymerization efficiency as well as fidelity.

The overall catalytic efficiency for 5-NIMP insertion opposite natural nucleobases is reduced between 1 and 3 orders of magnitude when compared to insertion opposite an abasic site. The K_d for 5-NITP is nearly identical whether or not a template nucleobase is present. These data have two important ramifications for polymerization catalyzed by gp43. The first point is that ground-state binding does not appear to play a large role in nucleotide discrimination. Instead, the conformational change step preceding phosphoryl transfer is most likely the parameter affected by the nature of the formed base pair. The second and perhaps more intriguing ramification is the potential for a "nonspecific" binding site for an incoming dNTP that takes advantage of $\pi-\pi$ stacking interactions between the aromatic rings of the incoming dNTP and amino acids. It will be of great interest

to evaluate if these phenomena are observed with other DNA polymerases or if they are unique to the phage enzyme.

A critical examination of the known structures of gp43 from bacteriophage RB69 (*52*−*54*) has provided a reasonable mechanistic explanation to account for the preferential insertion of 5-NIMP opposite the abasic site. A model is proposed invoking stabilization of the incoming nucleotide by $\pi-\pi$ stacking interactions of the aromatic moiety of the incoming nucleobase with several aromatic amino acids that line the polymerase's active site. An enzyme-mediated conformational change is proposed to move the triphosphate moiety of the nucleotide into close proximity of positively charged amino acids (enthalpic stabilization) while the aromatic nucleobase is transferred into the aromatic environment of the interior of the duplex DNA (entropic stabilization).

SUPPORTING INFORMATION AVAILABLE

Two figures showing pre-steady-state time courses comparing 5-NIMP insertion opposite template T or A and time courses comparing 5-NIMP insertion using $13/20_C$ or $13/20_G$. This material is available free of charge via the Internet at http://pubs.acs.org.

REFERENCES

1. Loeb, L. A., Springgate, C. F., and Battula, N. (1974) *Cancer Res. 34*, 2311−2321.
2. Knudson, A. G. (1996) *J. Cancer Res. Clin. Oncol. 122*, 135−140.
3. Schar, P. (2001) *Cell 104*, 329−332.
4. Mol, C. D., Parikh, S. S., Putnam, C. D., Lo, T. P., and Tainer, J. A. (1999) *Annu. Rev. Biophys. Biomol. Struct. 28*, 101−128.
5. Lawley, P. D., and Philips, D. H. (1996) *Mutat. Res. 355*, 13−40.
6. Sanderson, B. J. S., and Shield, A. J. (1996) *Mutat. Res. 355*, 41−57.
7. Lindahl, T. (1993) *Nature 362*, 709−715.
8. Lawley, P. D., Lethbridge, J. H., Edwards, P. A., and Shooter, K. V. (1969) *J. Mol. Biol. 39*, 181−198.
9. Pegg, A. E., and Byers, T. L. (1992) *FASEB J. 6*, 2302−2310.
10. Povirk, L. F., and Shuker, D. E. (1994) *Mutat. Res. 318*, 205−226.
11. Huang, J.-C., Hsu, D. S., Kazantsev, A., and Sancar, A. (1994) *Proc. Natl. Acad. Sci. U.S.A. 91*, 12213−12217.
12. Ioannidou, E., Lialiaris, T., Mourelatos, D., and Dozi-Vassiliades, J. (1989) *Mol. Mutagen 14*, 6−12.
13. Kow, Y. W. (2002) *Free Radical Biol. Med. 33*, 886−893.
14. Nelson, J. R., Lawrence, C. W., and Hinkle, D. C. (1996) *Science 272*, 1646−1649.
15. Masutani, C., Kusumoto, R., Iwai, S., and Hanaoka, F. (2000) *EMBO J. 19*, 3100−3109.
16. Zhang, Y., Yuan, F., Wu, X., Taylor, J. S., and Wang, Z. (2001) *Nucleic Acids Res. 29*, 928−935.
17. Schaaper, R. M., Kunkel, T. A., and Loeb, L. A. (1983) *Proc. Natl. Acad. Sci. U.S.A. 80*, 487−491.
18. Boiteux, S., and Laval, J. (1982) *Biochemistry 21*, 6746−6751.
19. Efrati, E., Tocco, G., Eritja, R., Wilson, S. H., and Goodman, M. F. (1997) *J. Biol. Chem. 272*, 2559−2569.
20. Mozzherin, D. J., Shibutani, S., Tan, C.-K., Downey, K. M., and Fisher, P. A. (1997) *Proc. Natl. Acad. Sci. U.S.A. 94*, 6126−6131.
21. Avkin, S., Adar, S., Blander, G., and Livneh, Z. (2002) *Proc. Natl. Acad. Sci. U.S.A. 99*, 3764−3769.
22. Berdis, A. J. (2001) *Biochemistry 40*, 7180−7191.
23. Vesnaver, G., Change, C. N., Eisenberg, M., Grollman, A. P., and Breslauer, K. J. (1989) *Proc. Natl. Acad. Sci. U.S.A. 86*, 3614−3618.
24. Gelfand, C. A., Plum, G. E., Grollman, A. P., Johnson, F., and Breslauer, K. J. (1998) *Biochemistry 37*, 7321−7327.
25. Sagi, J., Guliaev, A. B., and Singer, B. (2001) *Biochemistry 40*, 3859−3868.
26. Cuniasse, P., Sowers, L. C., Eritja, R., Kaplan, B., Goodman, M. F., Cognet, J. A. H., LeBret, M., Guschlbauer, W., and Fazakerley, G. V. (1987) *Nucleic Acids Res. 15*, 8003−8022.
27. Cuniasse, P., Fazakerley, G. V., Guschlbauer, W., Kaplan, B. E., and Sowers, L. C. (1987) *J. Mol. Biol. 213*, 303−314.
28. Hoehn, S. T., Turner, C. J., and Stubbe, J. (2001) *Nucleic Acids Res. 16*, 3413−3423.
29. Goodman, M. F., Ceighton, S., Bloom, L. B., and Petruska, J. (1993) *Crit. Rev. Biochem. Mol. Biol. 28*, 83−126.
30. Kool, E. T. (2001) *Annu. Rev. Biophys. Biomol. Struct. 30*, 1−22.
31. Matray, T. J., and Kool, E. T. (1999) *Nature 399*, 704−709.
32. Kuchta, R. D., Benkovic, P. A., and Benkovic, S. J. (1988) *Biochemistry 27*, 6716−6725.
33. Frey, M. W., Nossal, N. G., Capson, T. L., and Benkovic, S. J. (1993) *Proc. Natl. Acad. Sci. U.S.A. 90*, 2579−2583.
34. Rush, J., and Konigsberg, W. H. (1989) *Prepr. Biochem. 19*, 329−340.
35. Joyce, C. M., and Derbyshire, V. (1995) *Methods Enzymol. 262*, 3−13.
36. Johnson, K. A. (1995) *Methods Enzymol. 249*, 38−61.
37. Mizrahi, V., Benkovic, P. A., and Benkovic, S. J. (1986) *Proc. Natl. Acad. Sci. U.S.A. 83*, 5769−5773.
38. Capson, T. L., Peliska, J. A., Kaboord, B. F., Frey, M. W., Lively, C., Dahlberg, M., and Benkovic, S. J. (1992) *Biochemistry 31*, 10984−10994.
39. Caldwell, J. W., and Kollman, P. A. (1985) *J. Biomol. Struct. Dyn. 3*, 57−66.
40. Lin, P. K. T., and Brown, D. M. (1989) *Nucleic Acids Res. 17*, 10383.
41. Loakes, D., and Brown, D. M. (1994) *Nucleic Acids Res. 22*, 4039−4043.
42. Guckian, K. M., Schweitzer, B. A., Ren, R. X.-F., Sheils, C. J., Tahmassebi, D. C., and Kool, E. T. (2000) *J. Am. Chem. Soc. 122*, 2213−2222.
43. Moran, S., Ren, R. X., and Kool, E. T. (1997) *Proc. Natl. Acad. Sci. U.S.A. 94*, 10506−10511.
44. McMinn, D. L., Ogawa, A. K., Wu, Y. O., Shultz, P. G., and Romesberg, F. E. (1999) *J. Am. Chem. Soc. 121*, 11585−11586.
45. Chiaramonte, M., Moore, C. L., Kincaid, K., and Kuchta, R. D. (2003) *Biochemistry 42*, 10472−10481.
46. Minnick, D. T., Liu, L., Grindley, N. D., Kunkel, T. A., and Joyce, C. M. (2002) *Proc. Natl. Acad. Sci. U.S.A. 99*, 1194−1199.
47. Morales, J. C., and Kool, E. T. (2000) *J. Am. Chem. Soc. 122*, 1001−1007.
48. Matsuda, S., Henry, A. A., Schultz, P. G., and Romesberg, F. E. (2003) *J. Am. Chem. Soc. 125*, 6134−6139.
49. Searle, M. S., and Williams, D. H. (1993) *Nucleic Acids Res. 11*, 2051−2056.
50. Pyshnyi, D. V., Pyshnaya, I., Levina, A., Goldberg, E., Zarytova, V., Knorre, D., and Ivanova, E. (2001) *J. Biomol. Struct. Dyn. 19*, 555−570.
51. Wang, W., Wan, W., Zhou, H. H., Niu, S., and Li, A. D. (2003) *J. Am. Chem. Soc. 125*, 5248−5249.
52. Wang, J., Sattar, A. K., Wang, C. C., Karam, J. D., Konigsberg, W. H., and Steitz, T. A. (1997) *Cell 89*, 1087−1099.
53. Shamoo, Y., and Steitz, T. A. (1999) *Cell 99*, 155−166.
54. Franklin, M. C., Wang, J., and Steitz, T. A. (2001) *Cell 105*, 657−667.
55. Karam, J. D., and Konigsberg, W. H. (2000) *Prog. Nucleic Acid Res. Mol. Biol. 64*, 65−96.
56. Wang, C.-C., Yeh, L. S., and Karam, J. D. (1995) *J. Biol. Chem. 270*, 26558−26564.
57. Brautigam, C. A. and Steitz, T. A. (1998) *Curr. Opin. Struct. Biol. 8*, 54−63.
58. Beese, L. S., Derbyshire, V., and Steitz, T. A. (1993) *Science 260*, 352−355.
59. Beese, L. S., Friedman, J. M., and Steitz, T. A. (1993) *Biochemistry 32*, 14095−14101.
60. Doublie, S., Tabor, S., Long, A. M., Richardson, C. C., and Ellenberger, T. (1998) *Nature 391*, 251−258.

61. Doublie, S., and Ellenberger, T. (1998) *Curr. Opin. Struct. Biol. 8*, 704−712.
62. Braithewaite, D. K., and Ito, J. (1993) *Nucleic Acids Res. 21*, 787−802.
63. Bebenek, A., Dressman, H. K., Carver, G. T., Ng, S., Petrov, V., Yang, G., Konigsberg, W. H., Karam, J. D., and Drake, J. W. (2001) *J. Biol. Chem. 276*, 10387−10397.
64. Bebenek, A., Carver, G. T., Dressman, H. K., Kadyrov, F. A., Haseman, J. K., Petrov, V., Konigsberg, W. H., Karam, J. D., and Drake, J. W. (2002) *Genetics 162*, 1003−1018.
65. Gardner, A. F., and Jack, W. E. (1999) *Nucleic Acids Res. 27*, 2545−2553.
66. Spicer, E. K., Rush, J., Fung, C., Reha-Krantz, L. J., Karam, J. D., and Konigsberg, W. H. (1988) *J. Biol. Chem. 263*, 7478−7486.
67. Smerdon, S. J., Jager, J., Wang, J., Kohlstaedt, L. A., Chirino, A. J., Friedman, J. M., Rice, P. A., and Steitz, T. A. (1994) *Proc. Natl. Acad. Sci. U.S.A. 91*, 3911−3915.
68. Yang, G., Franklin, M., Li, J., Lin, T.-C., and Konigsberg, W. (2002) *Biochemistry 41*, 2526−2534.
69. Li, Y., Kong, Y., Korolev, S., and Waksman, G. (1998) *Protein Sci. 7*, 1116−1123.

BI034948S